The Institute of Space and Astronautical Science
Report No. 620, November 1986

Destruction Test of Small Scaled Solid Propellant Motors

By

Motoki HINADA, Ryojiro AKIBA, Teruo KISHI,
Yasunori MATOGAWA and Shigeki TSUKAMOTO

(July 10, 1986)

Summary: Destruction tests have been carried out on the ground by using three small scaled motors of solid propellant with a pair of destruction devices of V-shaped charge type. Each motor has the size of about 1/10 of the rear segment of one third of the 1st stage of Mu-3C that is a three staged and all solid propellant satellite launcher, developed by ISAS. Destruction devices in these tests are roughly the same in function and installation as those for Mu-3C. Several interesting results have been obtained on breakup characteristics of motor, such as mode of destruction, shapes of fragments of propellant and hardware, scattering distribution of them, shock load undergone by motor and surrounding overpressure. These results are expected to be useful for prediction of breakup characteristics of Mu-3C due to V-shaped charges.

1. INTRODUCTION

For flight safety operation, large rockets of ISAS, such as Lambda and Mu rockets, have the function of thrust termination in their powered flights by on-board destruction devices. Two different types of destruction devices are used in these rockets. One is so called V-shaped charge type that is attached to motor case. Initiating this will puncture the case and probably break up the vehicle itself. The other is a device of opening the end plate of motor opposite to its nozzle side by actuating separation nuts.

For example, Mu-3C which is a three staged and all solid propellant rocket and an advanced satellite launcher with radio guidance and control systems, developed after M-4S project, is equipped with these two kinds of destruction devices. The first stage has a pair of destruction devices of V-shaped charge type, whose explosive is the composition C4. These devices are attached to the rear part of the 1st stage motor case along its longitudinal axis, symmetrically to each other with respect to this axis. Destruction device of the 2nd stage is one of end plate opening type.

Several experiments on thrust termination of motor on ground and in flight by a device of the latter type have been carried out at Noshiro Testing Center and Kagoshima Space Center of ISAS, and the utility of this kind of device has been ascertained. On the other hand, breakup characteristics of motor due to V-shaped charge has not yet been made clear enough to be predicted quantitatively, although this characteristics is essential for pertinent consideration on flight safety operation of the 1st stage of Mu-3C, in particular, immediately after its launching.

This document is provided by JAXA.

Then in order to investigate this characteristics as quantitatively as possible, destruction tests of three small scaled motors with a pair of destruction devices of V-shaped charge type have been planned and successfully carried out. Many interesting results have been obtained on breakup characteristics of motor, such as destruction mode, shapes of fragments of propellant and hardware, scattering distribution, surrounding overpressure and shock load suffered by motor or its testing stand.

2. Configurations of Motor and Destruct Device

2.1 Motor

Three small scaled motors have been prepared. These have the same size except the thickness of their cylindrical cases, and are 300 mm in length and 150 mm in diameter. Two of them have cylindrical cases of thickness of 1 mm and another does the one of thickness of 2 mm. Since breakup characteristics of motor due to V-shaped charge is thought to be influenced essentially by motor's configuration, rather much stress has been placed upon simulating the configuration of small motors in this experiment to that of the 1st stage motor of Mu-3C. Small motors are roughly similar to the rear segment of one third of the 1st stage motor of Mu-3C, and are in a scale of about 1/10 of that segment, while the thickness of cylindrical cases is 1/5–2/5 of the thickness of motor case of that segment. Cylindrical cases of these motors are made of nearly the same material as the one used for the motor case of Mu-3C, that is, high tensile maraging steel named HT-200.

One of motors with their cases of thickness of 1 mm and another motor with the one of thickness of 2 mm are loaded with the propellant, named BP-27B, and they have a sonic nozzle at their respective one end. Predicted values of burning time and average chamber pressure of these motors are 5 seconds and 50 kg/cm^2, respectively. Remainder motor is loaded with no propellant and then the end of its nozzle side is closed with a thick steel plate. Destruction test of this has been done on the condition that the chamber is pressurized with supply of nitrogen gas up to about the same levels as that of average chamber pressure of propellant loaded motors.

Configuration and principal parameters of testing motors are presented in Fig. 1 and Table 1, and a piture of testing motor is shown in Fig. 2.

2.2 Destruction device

Destruction device used in this experiment is the one of V-shaped charge type and like a rod with the length of 60 mm. Charged explosive of it consists of the composition C4 of 0.036 kg in weight, and has cross section like a V-shape, as shown in Fig. 1. This device and the one for the 1st stage motor of Mu-3C are almost the same, in configuration and function. They have an identical shape of cross section. Only a difference between them is that the length of the former is reduced to a scale of 1/5 of the latter's.

For each of testing motors a pair of destruction devices are installed on the cylindrical motor case, on the side opposite to the nozzle side of motor, along its longitudinal axis and symmetrically with respect to this axis, as shown in Fig. 2. Configuration and principal parameters of destruction device are included in Fig. 1 and Table 1.

This document is provided by JAXA.

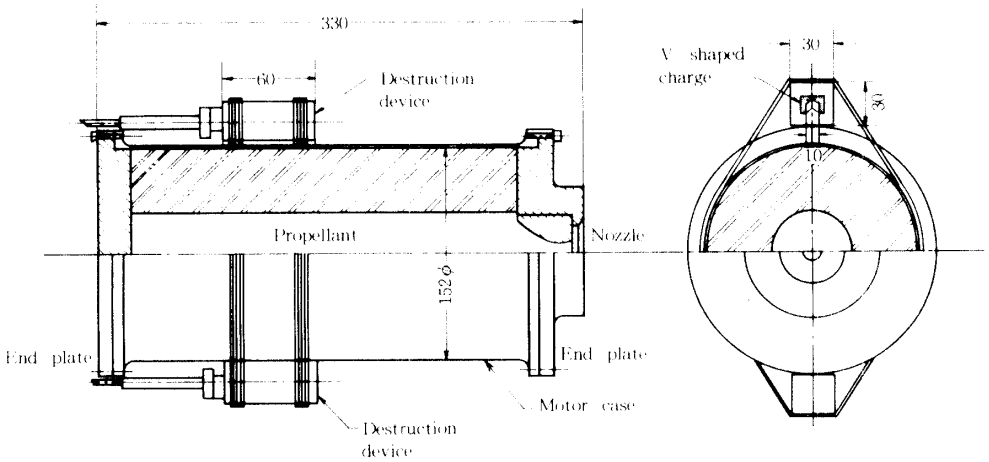

Fig. 1. General drawing of small scaled testing motor with a pair of destruction devices.

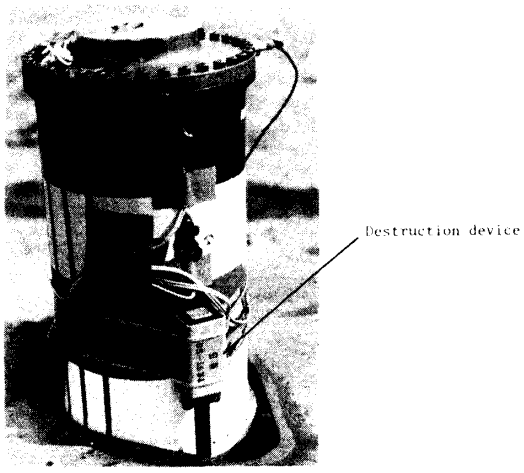

Fig. 2. A Picture of a Motor with Destruction Devices.

3. Procedure of Experiment

Ground tests of destruction of small scaled motors have been done at Noshiro Testing Center that belongs to ISAS and is localed at the coast near Noshiro City of Akita Prefecture in Japan. For this experiment a small testing stand to hold a motor vertically has been settled, as shown in Fig. 3, at some site of this center which is at the distance of 100 m even from the nearest construction to itself. A schematic view of the stand with a testing motor and a picture of it are shown in Fig. 4 and 5, respectively. As shown in these figures, the testing motor is placed on the stand vertically with its nozzle side upward and connected with the stand through a load cell to measure thrust of motor and longitudinal shock load due to V-shaped charges.

Three motors have been tested in the order of No. 1, 2 and 3 motors listed in Table 1. No. 1 motor have been tested on the condition that the chamber is pressurized up to 56 kg/cm^2 with supply of nitrogen gas. No. 2 and 3 motors have been tested at 1.5 seconds after their ignitions.

This document is provided by JAXA.

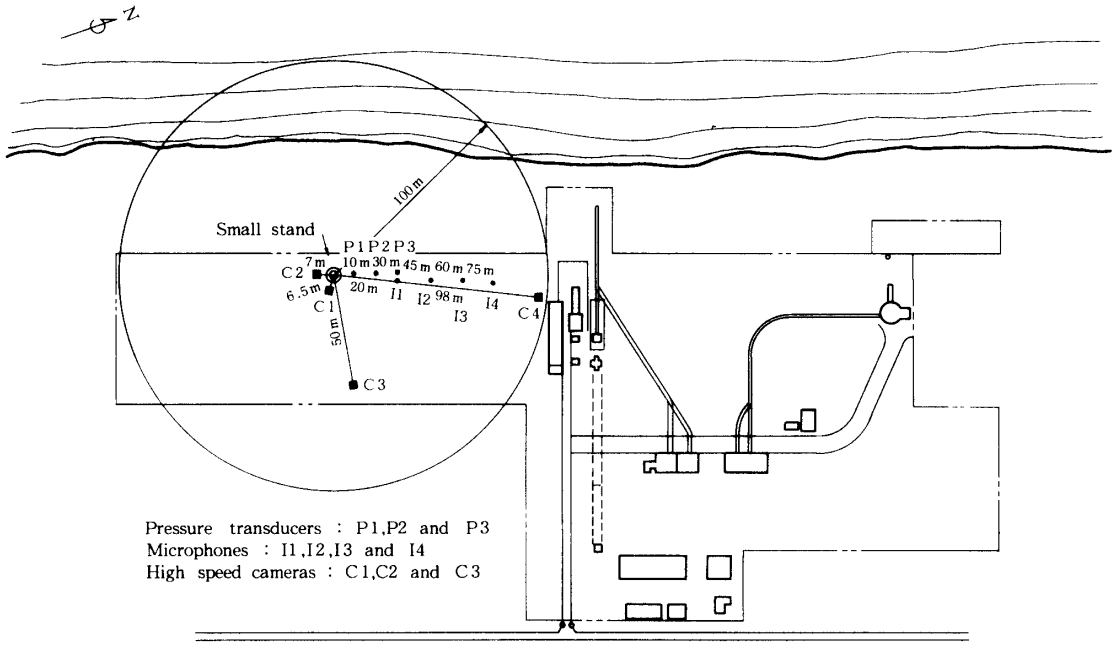

Fig. 3. General drawing of Noshiro Testing Center, including setting places of pressure transducers, microphones and high speed cameras.

Table 1. Principal Parameters of Motor Cases and Destruction Devices

Motor No.	Motor				Destruction Devices		
	Dimension of Case	Material of Case	Thickness of Case	Propellant	Dimension	Weight	Explosive
1	150 mm ϕ ×300 mm	Maraging Steel	1 mm	Non	600 mm	0.036 ×2= 0.072 kg	Composite C4
2			1 mm	BP-27B 4.8 kg			
3			2 mm				

4. Measurement

4.1 Thrust and longitudinal shock load

In order to measure thrust of motor and longitudinal shock load undergone by motor at the initiation of destruction devices, three kinds of load cells have been ready to be utilized. Their respective maximum levels of load are 0.3, 1 and 15 tons. Load cell is installed between the testing motor and the stand, connecting them together, as shown in Fig. 4. Load cells with smaller maximum levels of 0.3 and 1 tons have been used in the first and second tests, respectively. The one with largest maximum level has been used only in the final test.

This document is provided by JAXA.

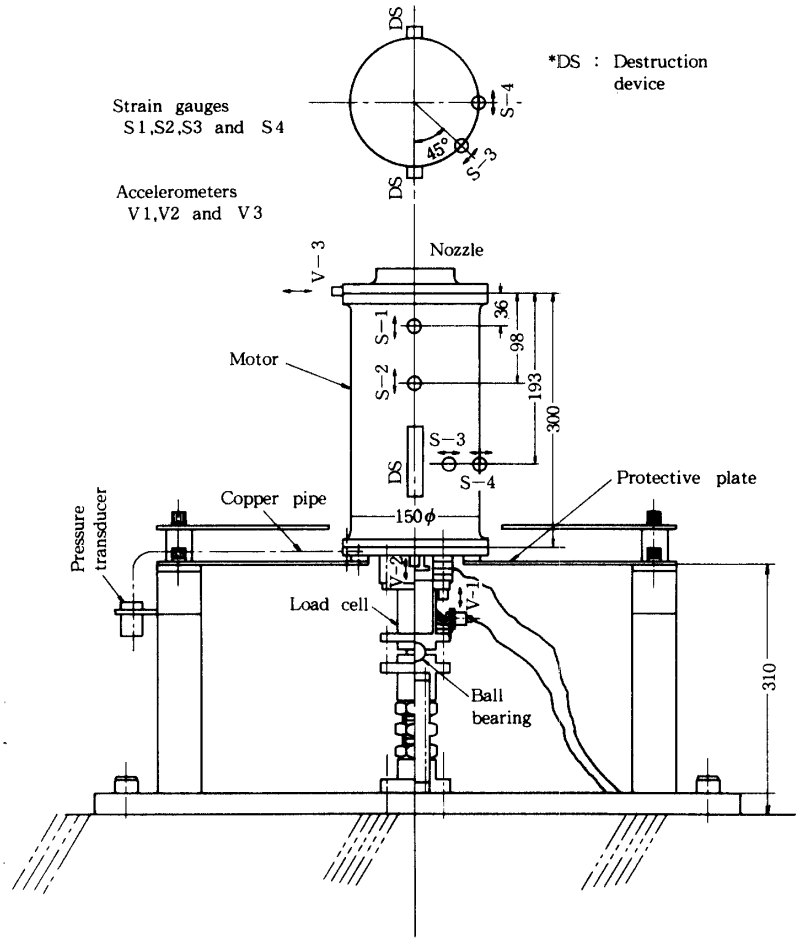

Fig. 4. Schematical drawing of a small stand with a testing motor set on it.

Table 2. Operating Conditions of High-speed Cameras

Camera	Lens (m/m)	Image Angle		Frame Speed (sec)	Shutter Speed (sec)
		Vertical	Horizontal		
No. 1	150	2.8°	3.8°	5000	1/25000
No. 2	135	3.5°	4.6°	5000	1/25000
No. 3	20	20.8°	28.7°	1000	1/5000
No. 4	25	16.7°	23.1°	500	1/1500

This document is provided by JAXA.

4.2 Acceleration shock

Shock suffered by motor and it's testing stand also has been investigated by use of three accelerometers of piezo type. These sensors labeled as V1, V2 and V3 are mounted on both motor and load cell, as shown in Fig. 4, and these aim to measure longitudinal and transversal accelerations.

4.3 Strain

In order to examine the characteristics of stress wave and fracture propagating on cylindrical motor case due to V-shaped charges, strain of cylindrical case has been measured by use of strain gauges. Four strain gauges labeled as S1, S2, S3 and S4 are struck on each cylindrical case around one of destruction devices, as shown in Fig. 4. Two gauges, S1 and S2 are in a row of circumferential direction and aim to measure longitudinal strain, while other two, S3 and S4 are in a row of longitudinal direction and aim to measure circumferential strain. This measurement system has the frequency response up to 10 kHz, and is capable of sensing transient behavior of stress wave or fracture if it propagates with velocity less then 1 kg/sec.

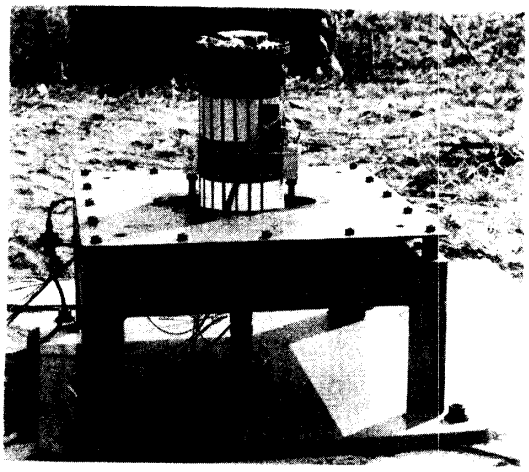

Fig. 5. Picture of a small stand with a testing motor set on it.

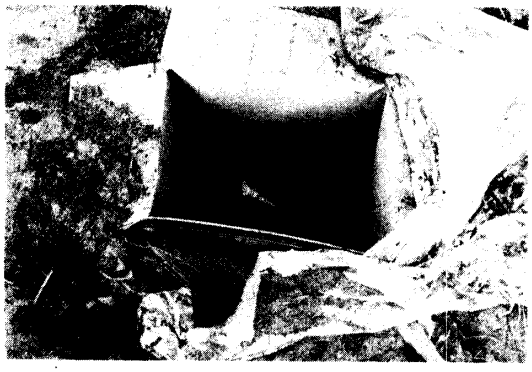

Fig. 6. Setting method of microphone.

This document is provided by JAXA.

4.4 Chamber pressure

Measurement of chamber pressure has been done with a pressure transducer of strain gauge type. As shown in Fig. 4, this sensor is connected with the end plate of motor opposite to its nozzle side, through a copper pipe with length of 600 mm and diameter of 6 mm.

4.5 Overpressure of shock wave and intensity of sound wave

Overpressure of shock wave and intensity of sound wave in the surroundings of testing motor have been measured with three pressure transducers of semi-conductor type and four high sensible microphones of conductance type, respectively. These sensors are placed at the distance of 10–75 m from the stand, as shown in Fig. 3. Pressure transducers labeled as P1, P2 and P3 are at rather nearer sites to the stand, and these are to measure static overpressure of shock wave produced by destruction of motor. Microphones labeled as I1, I2, I3 and I4 are at rather far distance from the stand, and these are to measure intensity of sound wave due to motor destruction. Each microphone is set in a box ($30\times40\times30$ cm) which is buried in the ground with its upper side open, and this setting method is shown in Fig. 6.

5. Optical Observation

Optical observation on both phenomena of propagation of fracture on motor case and scattering aspect of fragments of propellant and hardware has been tried by use of four high speed cameras. These cameras labeled as C1, C2, C3 and C4 are set at different sites in the surroundings of the stand, as shown in Fig. 3. Two cameras, C1 and C2 aim to observe the propagation of fracture on motor case and are at the distance of about 7 m from the stand. They take different views of motor with their full image angles and both are driven with the same speed of 5000 frames/sec. View taken by camera C1 is a nearly symmetrical one with respect to one of destruction devices, while view by camera C2 is a side one roughly normal to this.

On the other hand, cameras C3 and C4 have an objective to observe the scattering aspect of fragments of propellant and hardware, such as cylindrical motor case and end plate with or without nozzle. These cameras are at the distances of 50 m and 98 m from the stand and are operated with the speeds of 1000 and 500 frames/sec, respectively.

Operating conditions of high speed cameras in this experiment are shown in Table 2.

6. Experimental Results

No. 1, 2 and 3 motors have been tested in this order. Tests have made clear the breakup characteristics of motor due to V-shaped changes, quantitatively to some extent, and they have accomplished their objectives successfully. The following several results have been obtained from this experiment.

6.1 Chamber pressure

No. 1 motor has been tested after its chamber has been pressurized up to 56 kg/cm^2 with supply of nitrogen gas. No. 2 and 3 motors have been tested at 1.5 seconds after their ignitions,

This document is provided by JAXA.

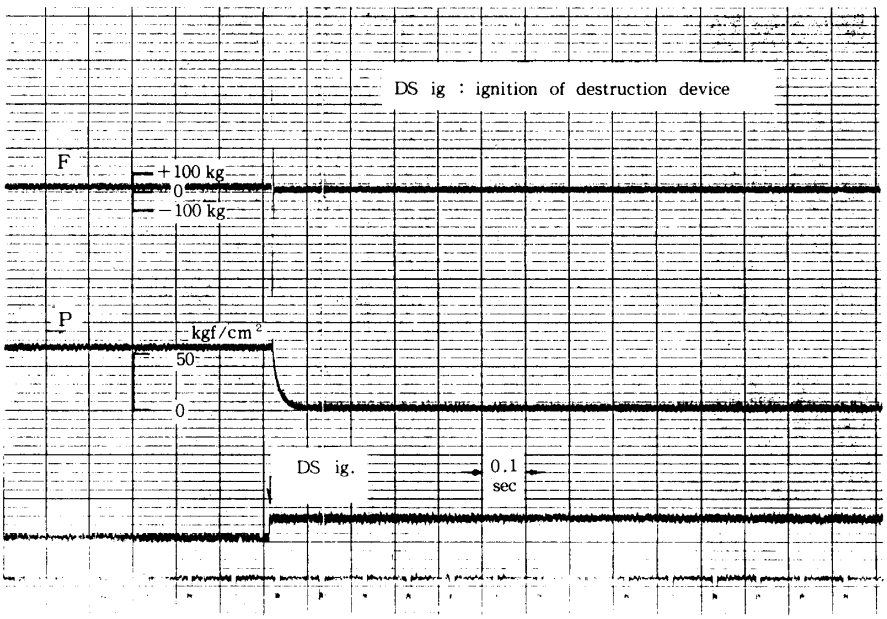

Fig. 7. (a) Results of chamber pressure, P, and longitudinal shock load, F, for 1st test.

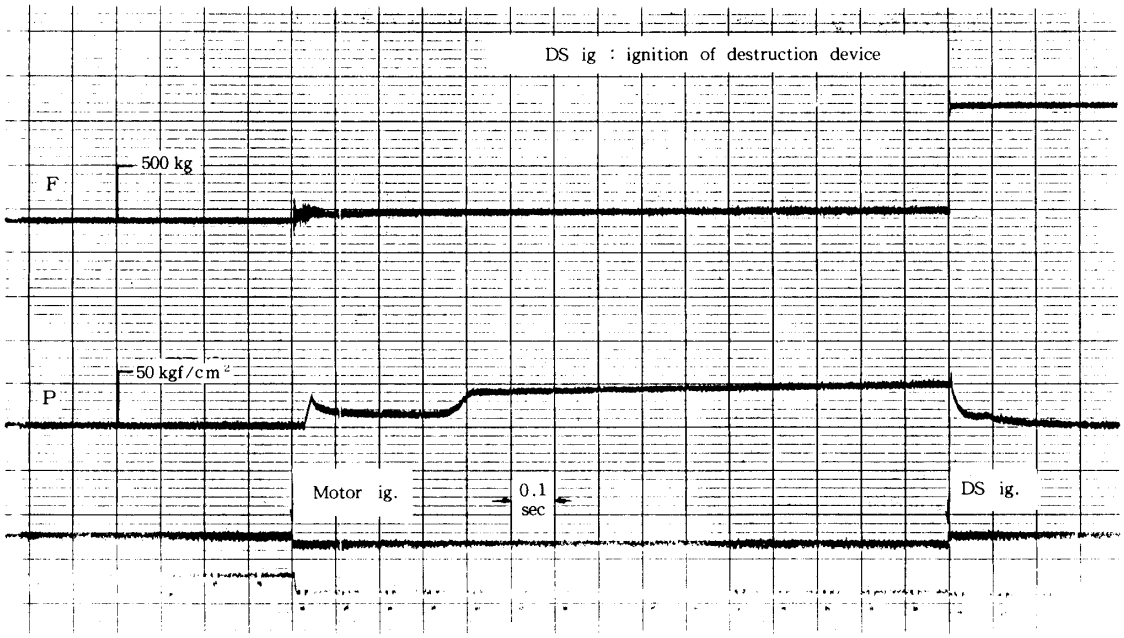

Fig. 7. (b) continued, for 2nd test.

when their respective chamber pressures have risen to about 36 kg/cm^2. Time histories of chamber pressure, designated by P, are presented in Fig. 7, in which time histories of thrust or longitudinal shock load, designated by F, are also included. It is found from Fig. 7 that respective chamber pressures are reduced to the atmospheric pressure in about 50 msec and that these trends of pressure reduction are nearly the same, independent of both the thickness of motor case and the condition whether motor is loaded with propellant or not. Comparatively gradual reduction of measured chamber pressures is a contrast to more sharp reduction

This document is provided by JAXA.

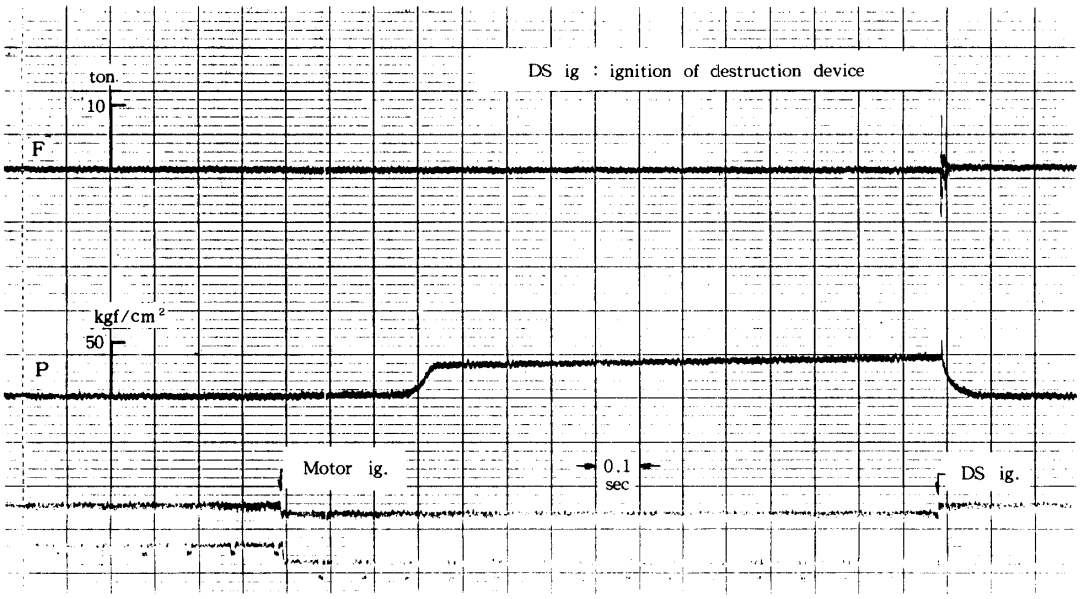

Fig. 7. (c) continued, for 3rd test.

presumed from aerodynamic theory. This reason is probably due to the fact that in this experiment chamber pressure has been measured through a fine pipe having the length of 60 cm.

6.2 Longitudinal shock load

Longitudinal shock load obviously depends on destruction mode of motor case. In the first test, the load cell with maximum level of 0.3 ton has been used on the supposition that motor case would be punctured partially just around a pair of destruction devices. Actual scale of destruction, however, has been larger than the supposed one, as will be explained below. Longitudinal shock load has been beyond capability of the load cell used. Then the load cell with larger maximum level of 1 ton has been used in the second test, where longitudinal shock load also has been beyond load cell capability. In the final test, therefore, the load cell with largest maximum level of 15 ton has been utilized and has been able to measure longitudinal shock load successfully. Measured maximum value of longitudinal shock load is 9.8 ton. This value is nearly equal to the quantity that is given by multiplying a dynamic load factor of 2 and the product of cross sectional area of cylindrical motor case (154 cm^2) and chamber pressure just before the initiation of destruction devices (36 kg/cm^2). This suggests that the cylindrical motor case has been cut off by completely circumferential fracture. Time histories of thrust or longitudinal shock load, designated by F, are presented in Fig. 7.

6.3 Acceleration shock

Attempts of measuring longitudinal and transversal acceleration shocks have been unsuccessful in all tests. This reason is that these shocks have been so fast and so large that accelerometers of piezo type used in the present experiment have been unsuitable to sense them normally and quantitatively.

This document is provided by JAXA.

6.4 Strain

Results on strain of motor case are presented in Fig. 8, which shows the following. In each test, four strain gauges have sensed quantities of strain corresponding accurately to the chamber pressure till the initiation of destruction devices. These gauges have caught some respective variations of strain at almost the same time, 4 msec after the initiation signal of destruction devices, and then output of these sensors has been saturated within 1 msec. The time lag of 4 msec is thought to correspond mostly to the time from the initiation signal to the actual initiation. The difference between the times at which respective strain gauges have caught the initial variations of strain that are probably produced by the first stress wave due to V-shaped charges seems to be less than 0.1 msec. This may mean that actual propagating velocity of stress wave or fracture is comparatively large than 1 kg/sec.

6.5 Overpressure of shock wave and intensity of sound wave

Overpressure of incident shock wave that is caused by destruction of motor and propagates into surrounding air and intensity of sound wave following the shock wave have been measured successfully in all tests. As examples, results of them in the third test are presented in Fig. 9 and 10, from which it can be seen that the incident shock speed has been mostly reduced to that of sound wave at the distance of 10 m from the stand and that the sound wave due to motor destruction has lasted during about 0.3 sec with comparatively high intensity. Maximum value of static overpressure of incident shock wave that is measured by sensor P1 at the distance of 10 m from the stand is in the range of 0.012–0.015 kg/cm^2 for all tests. This value is approximately equal to that given by Sutton's formula when weight of gas in the chamber is used as equivalent TNT weight in this formula.

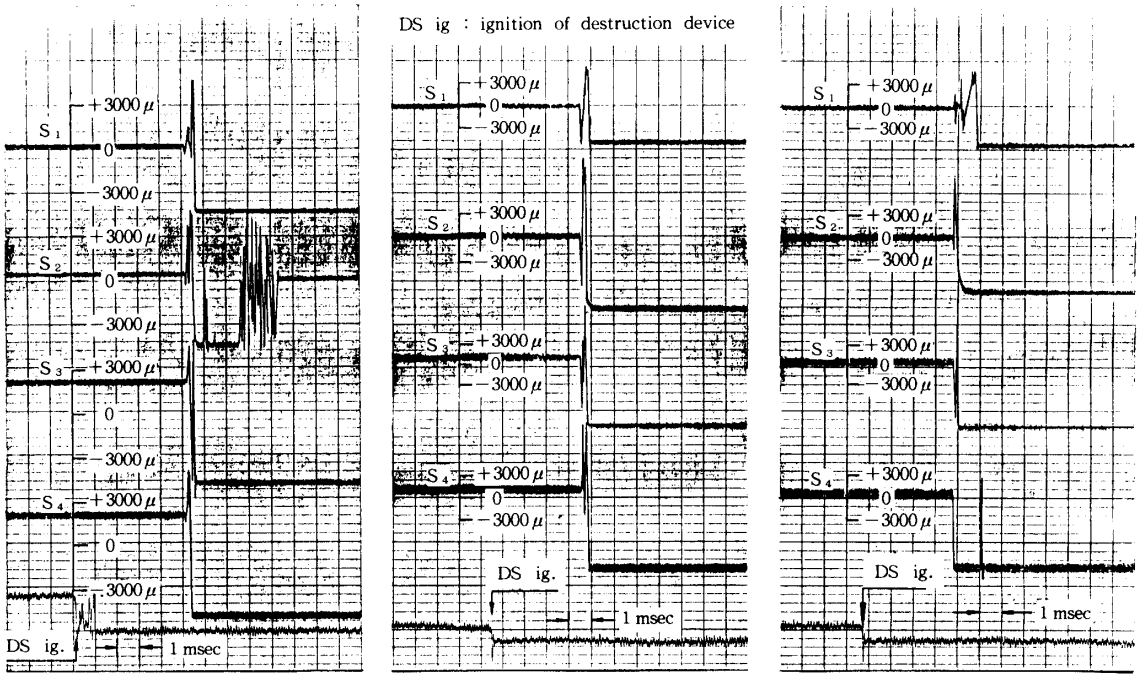

(a) 1st test (b) 2nd test (c) 3rd test

Fig. 8. Results on strain of motor case, measured by strain gauges, S1, S2, S3 and S4.

This document is provided by JAXA.

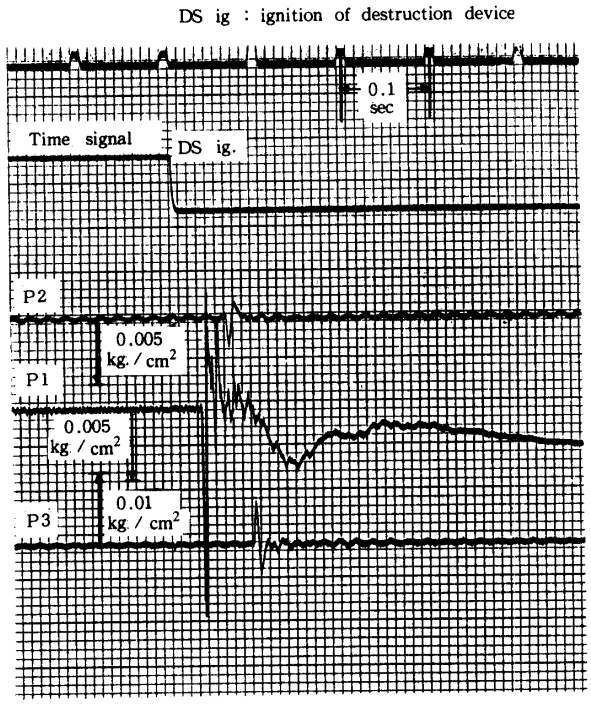

Fig. 9. Results of overpressure, measured by pressure transducers, P1, P2 and P3, for 3rd test.

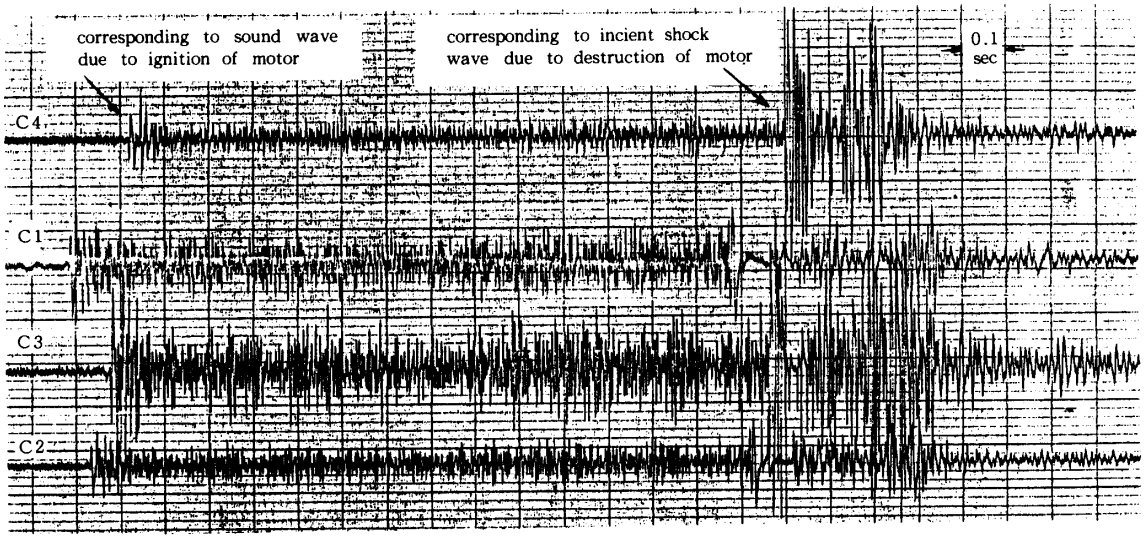

Fig. 10. Results of intensity of sound wave, measured by microphones, L1, I2, I3 and I4, for 3rd test.

6.6 Optical observation

For all tests, films of cameras C1 and C2 have given no distinct picture of bursting motor during about fifty frames after the initiation of destruction devices. This reason is that during these frames, high intensity of light due to the explosion of V-shaped changes has made halation occur on the films and then smoky gas following the explosion has made images on the films vague. After these frames, the films have given comparatively clear pictures of thrown-out fragments, as shown in Figs. 11 and 12. Consequently, it is possible that the initial

This document is provided by JAXA.

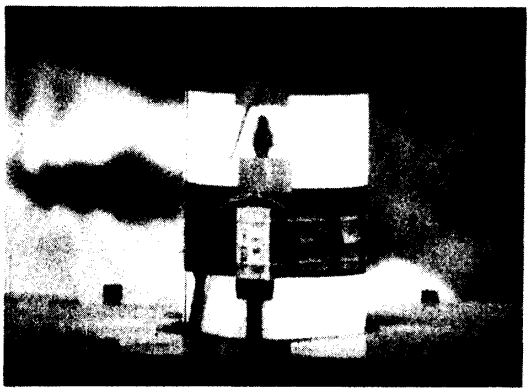

(a) No. 0 frame, just before destruction

(b) No. 77 frame

Fig. 11. Pictures taken by camera C1 with driving speed of 5000 frames/sec, for 1st test.

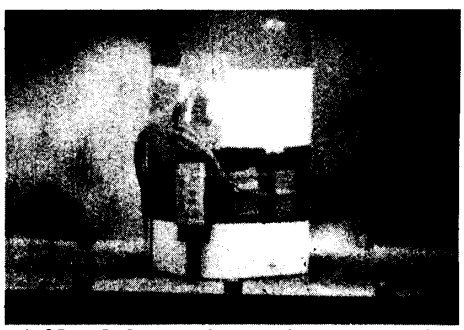

(a) No. 0 frame, just before destruction

(b) No. 69 frame

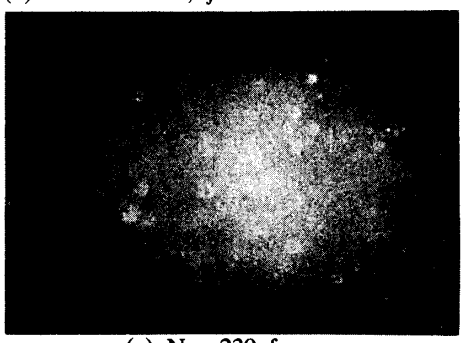

(c) No. 239 frame

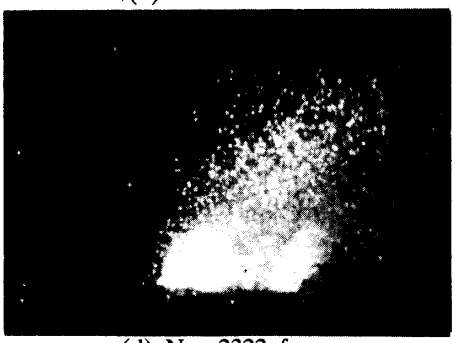

(d) No. 2322 frame

Fig. 12. Pictures taken by camera C1 with driving speed of 5000 frames/sec, for 3rd test.

This document is provided by JAXA.

(a) No. 0 frame, just before destruction

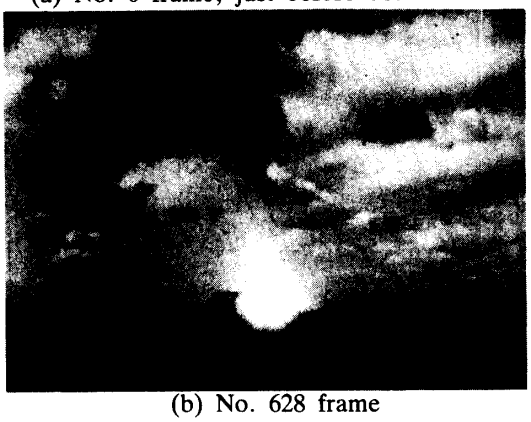

(b) No. 628 frame

(c) No. 872 frame

Fig. 13. Pictures taken by camera C3 with driving speed of 1000 frames/sec, for 3rd test.

thrown-out aspect of fragments is made comparatively clear by these films, although it is impossible to examine the detailed propagating aspect of fracture by using the films. At the present time, these films are being analyzed and the results of them will be obtained soon. As rough results, it seems that there have been some fragments which have been thrown out with such a fast initial velocity as 100–200 m/sec.

On the other hand, films of cameras C3 and C4 have made clear the thrown-out aspect of fragments of relatively large size. Some examples are presented in Fig. 13. Tracing these fragments gives that maximum value of the initial thrown-out velocity of them is approximately equal to 200 m/sec.

This document is provided by JAXA.

6.7 Recovering of fragments

After each test, laborious and eager efforts have been made to recover fragments scattered in the surrounding wide field around the destruction point. For the first test, the following pieces have been found, that is, the end plate on the upper side of motor, two large pieces of cylindrical case, and seven small fragments of cylindrical case and destruction devices. The end plate, as it was, has falled just near the stand. The two large pieces, which have the size of about a half of the original cylindrical case and can mostly reproduce it's original shape by themselves, have fallen at some places which are at the distance of about 10 m from the stand and on both sides of a line passing through a pair of destruction devices. Seven small fragments have been scattered within the distance of 20 m from the stand. The scattering aspects of metallic pieces for the second and third tests have been almost the same as the one for the first test. For the second and third tests, besides metallic pieces, many small fragments of propellant and restrictor have been recovered. Scattering aspect of fragments for the second test and that for the third test are presented in Figs. 14 and 15, respectively, which do not include end plate and two large pieces of cylindrical case. As found from Figs. 14 and 15, small fragments have been scattered widely, within the distance of 80 m from the stand. Some examples of recovered fragments are shown in Fig. 16.

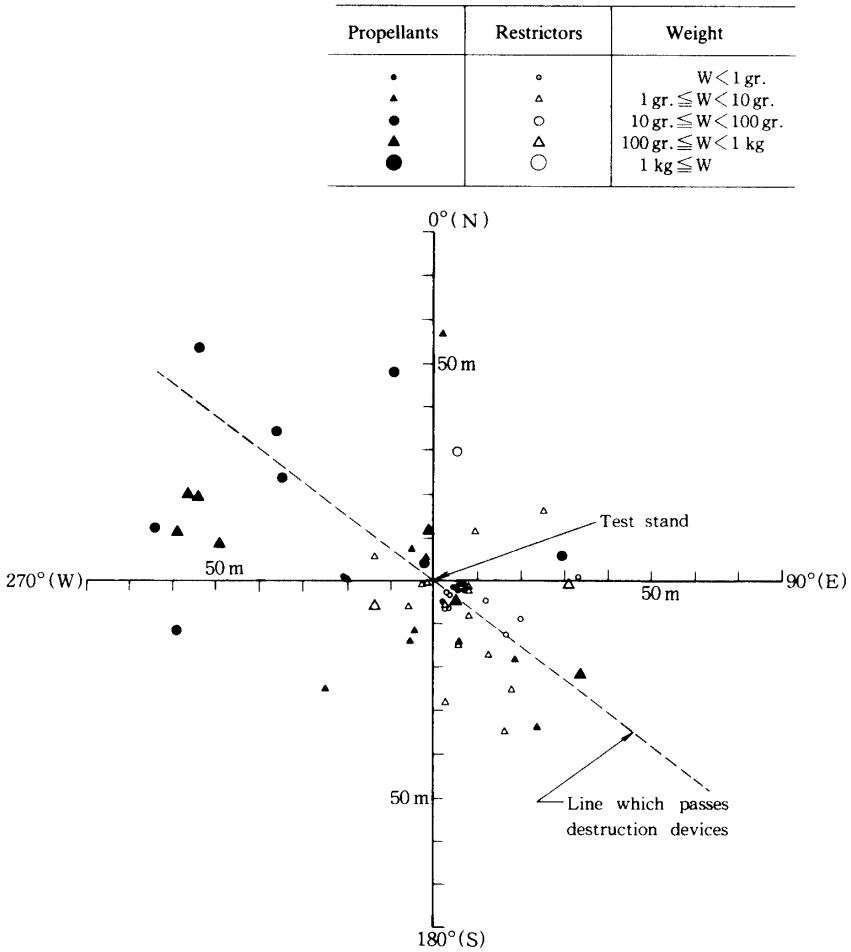

Fig. 14. Scattering Diagram of Fragments for 2nd Test.

This document is provided by JAXA.

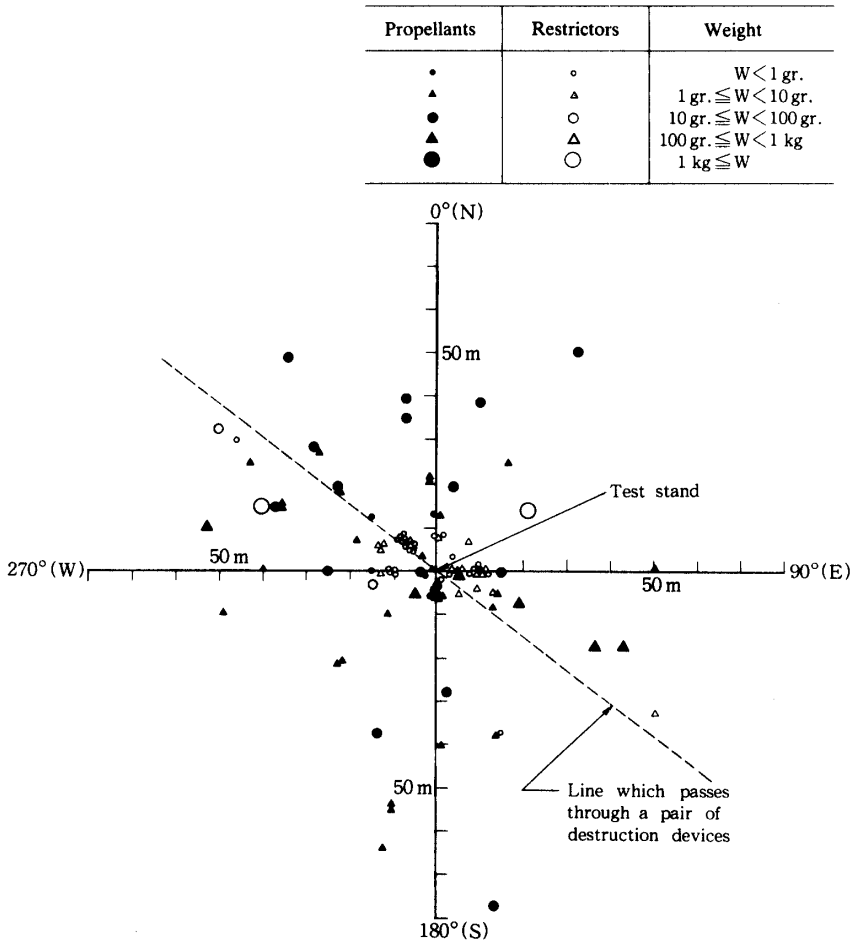

Fig. 15. Scattering Diagram of Fragments for 3rd Test.

As for small fragments except end plate and two large pieces of cylindrical case, the following results have been obtained. For the second test, the largest and smallest among fragments of propellant are 18 and 0.8 cm in maximum diameter, respectively, and the heaviest and lightest are 565 and 0.24 gr in weight, respectively. For the third test, the largest and smallest are 16 and 0.3 cm in maximum diameter, respectively, and heaviest and lightest are 412 and 0.27 gr in weight, respectively. Number distributions of fragment against its weight for the second and third tests, are shown in Figs. 17 and 18, and cumulative number distributions of fragment against distance from the stand for these tests are also shown in Figs. 19 and 20.

6.8 Fracture mode

Fracture modes of testing motors have been examined with recovered fragments. It has been found that as for the first and second motors with cylindrical case of thickness of 1 mm, their fracture modes are almost the same. It has been also found that there is some difference between the fracture mode of the third motor with cylindrical case of thickness of 2 mm and those of the first and second motors. As examples, fracture modes for the second and third motors are represented in Figs. 21 and 22, schematically and photographically. As shown in Fig. 21, fractures propagate initially along two longitudinal lines passing through destruction devices and then turn to propagate circumferentially near connecting parts of both end plates

This document is provided by JAXA.

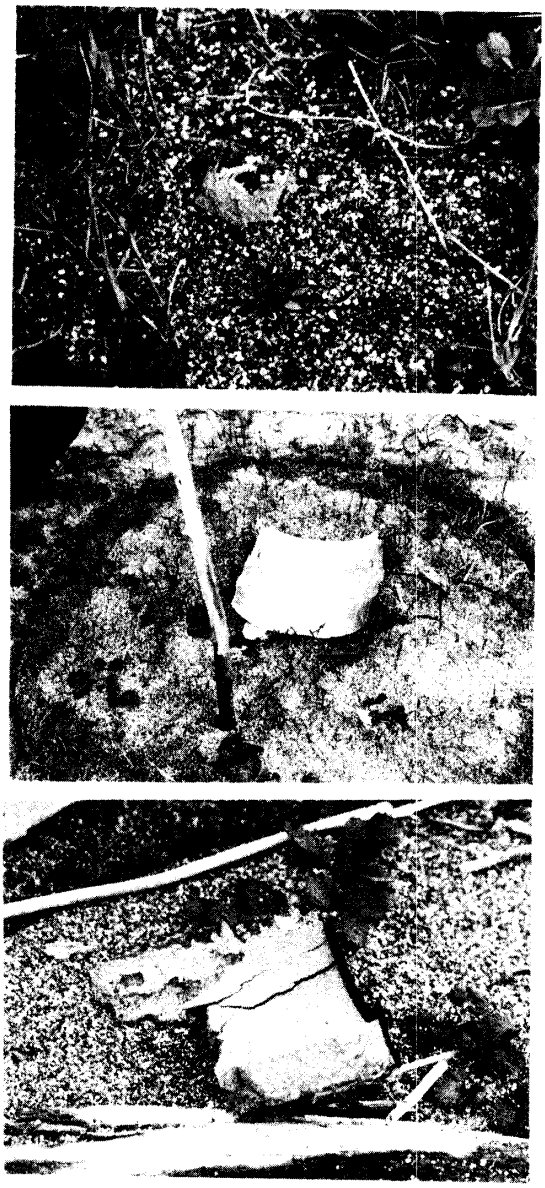

Fig. 16. Some pictures of recovered fragments.

and cylindrical case. In Fig. 21, the mark of arrow designates the propagating direction of fracture. It seems that the fracture modes of the first and second cases are ductile fractures, and the one of the third case is a quasi-brittle fracture. As shown in Fig. 21, welded parts of the second case are foul partly. This may be due to a ductile fracture of this case. It is thought that the first and second cases have suffered the large amount of strain before fractures propagate, owing to ductile fractures of these cases. Figure 23 shows the result of hardness of two fractured cases along the direction normal to fracture. As seen in this figure, fractured case with thickness of 1 mm is highly work hardened in the neighborhood of fracture surface. This figure confirms that destruction mode of case with thickness of 1 mm is a ductile fracture and the one of case with thickness of 2 mm is a quasi-brittle fracture. Difference between these destruction modes is also confirmed with the fractography by an electron microscope.

This document is provided by JAXA.

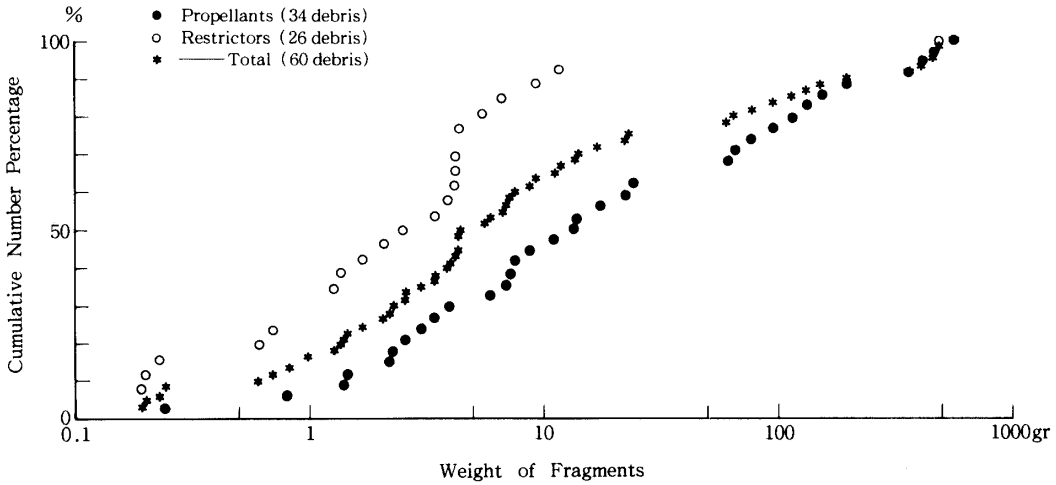

Fig. 17. Cumulative Number Distribution of Fragments against Their Weight (2nd Test).

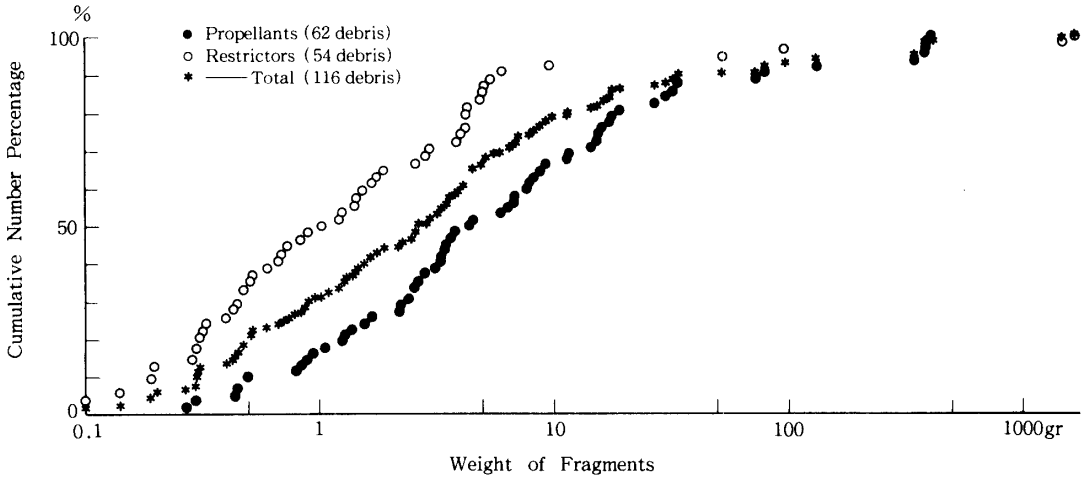

Fig. 18. Cumulative Number Distribution of Fragments against Their Weight (3rd Test).

Analysis of linear fracture mechanics gives, that the thickness of case should be more than 1.3 mm as a plane strain condition. Thickness of the first stage motor case of Mu-3C is 5 mm, and it satisfies this condition. Case of thickness of 2 mm also satisfies this condition. In this sense, fracture mode for the third motor can simulate that for the 1st stage of M-3C to some extent. The case of thickness of 1 mm, however, is in the condition of plane stress state and do not satisfy that condition.

This document is provided by JAXA.

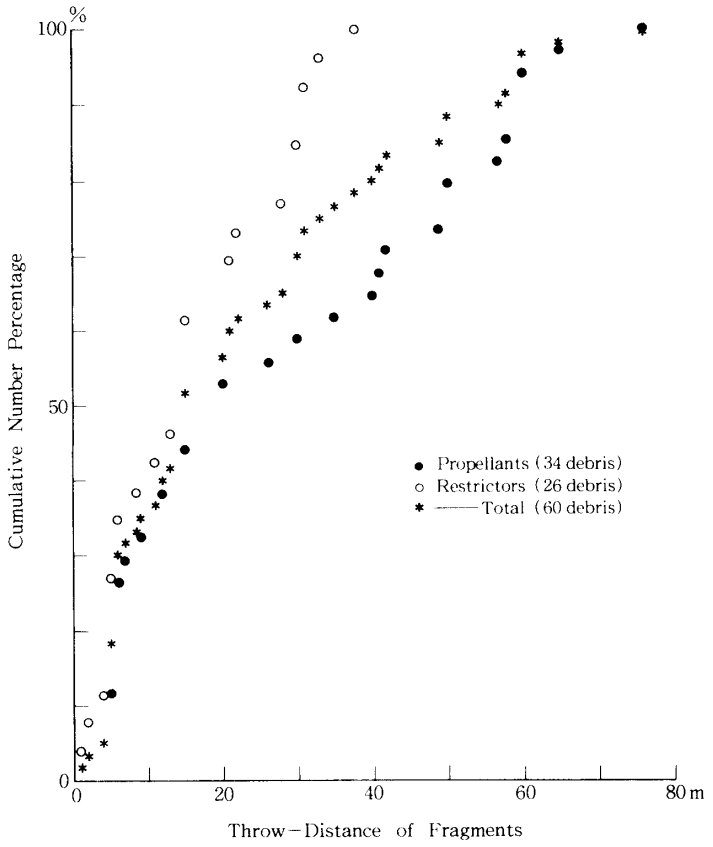

Fig. 19. Cumulative Number Distribution of Fragments against Their Throw-Distance (2nd Test).

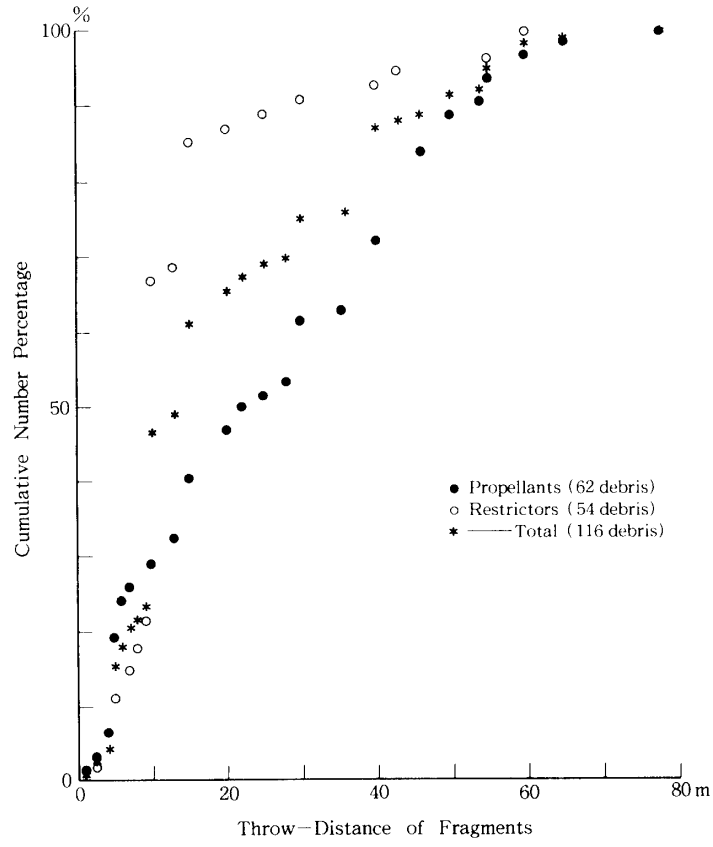

Fig. 20. Cumulative Number Distribution of Fragments against Their Throw-Distance (3rd Test).

This document is provided by JAXA.

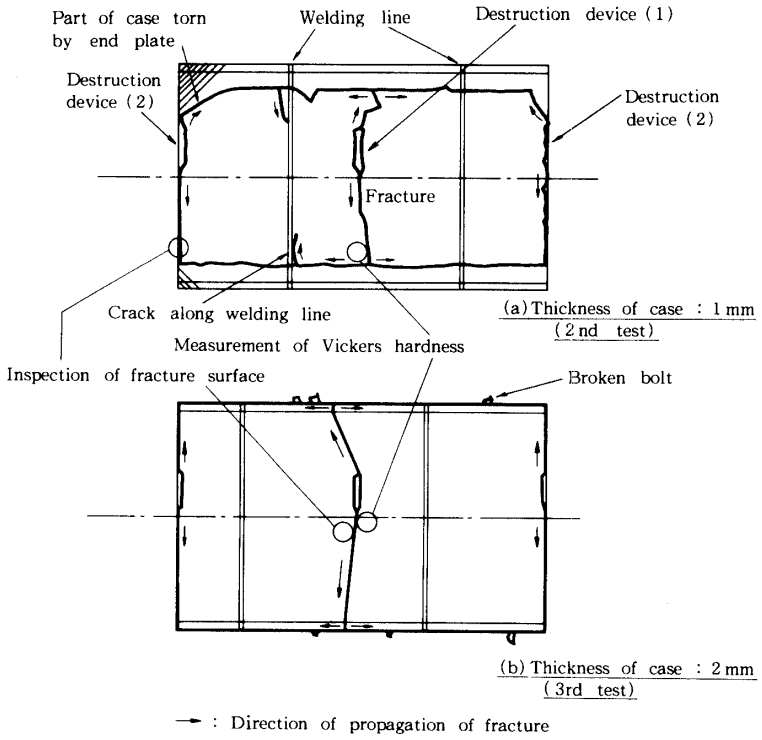

Fig. 21. Destruction modes for case of thickness.

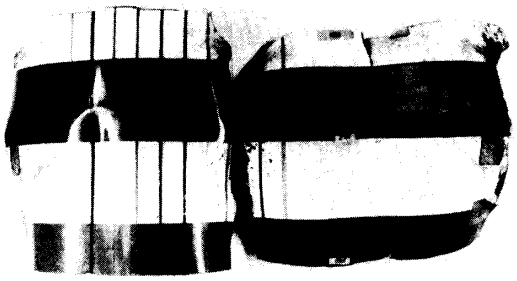

(a) Thickness of case: 1 mm, for 2nd test

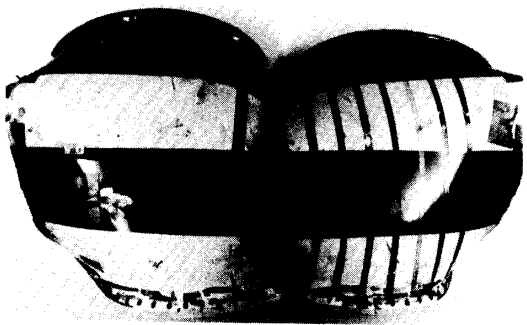

(b) Thickness of case: 2 mm, for 3rd test

Fig. 22. Two large pieces of cylindrical case, for 2nd and 3rd tests respectively.

This document is provided by JAXA.

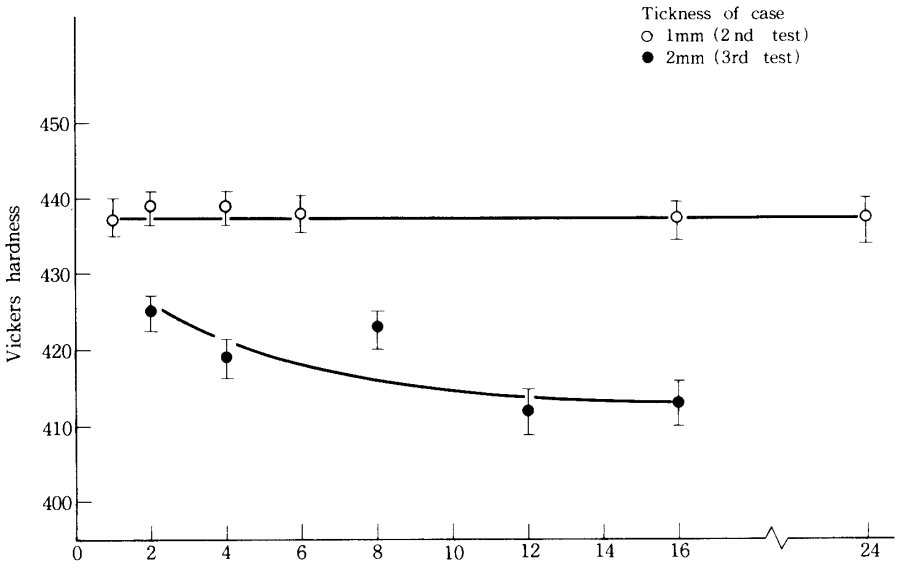

Fig. 23. Vickers hardness of broken cases for 2nd and 3rd tests.

This document is provided by JAXA.